Performance of Wells Turbines for use in Small-Scale Oscillating Water Columns

David G. Dorrell[1] and Min-Fu Hsieh[2]
[1]Dept. Electronics and Electrical Engineering, University of Glasgow
Glasgow, G12 8LT, UK
[2]Department of Systems and Naval Mechatronic Engineering, National Cheng Kung University
Tainan 701, Taiwan

ABSTRACT

This paper will assess the viability of small Wells turbines for oscillating water columns. The paper reports on a complete assessment of the integration of the system. It begins with a study using computational fluid dynamic analysis of a small double stage turbine. The analysis is carried though to assess performance under reciprocating airflow conditions. Experimental data will be put forward from the mounting of a turbine on a small-scale oscillating water column. The turbine will be connected to a DC machine to act as the generator for the system. While the system is simply a demonstrator, information about the column dynamics and turbine sizing is obtained.

KEY WORDS: Oscillating Water Column, Wells Turbine, Computational Fluid Dynamics

INTRODUCTION

Background

There is now a proliferation of different wave energy devices that are under investigation. These were briefly reviewed by Halliday ad Dorrell, 2004 and further explored by Dorrell and Hsieh, 2007. They can be broken down into five basic technology groups (Clement *et al*, 2002): oscillating water columns (OWC); overtopping devices; point absorbers (floating or mounted on the sea bed); surging devices; and mechanical extraction.

This paper is concerned with the oscillating water column (OWC) in conjunction with a Wells turbine. This is a very straightforward device and one that has been tried by several research groups and countries (including the UK, Japan, Portugal, Norway, and several others). An example is illustrated in Fig. 1 and it consists of two basic components: the chamber and the turbine. Waves flow into the front of the chamber so that the water level inside oscillates with a height and phase difference with respect to the wave fronts. This pressurises and depressurises the column so that air moves in and out of the chamber via a bidirectional turbine. Dorrell and Hsieh, 2007 tested a Savonius rotor turbine whereas here we will test a Wells turbine. Both of these turbines are illustrated in Fig. 1.

In most OWCs the turbine is a Wells type; these have pear-shaped blades that have the same rotation whatever the airflow direction is. They can have reasonable conversion rates provided the flow coefficient (inlet air velocity/turbine blade tip-speed) is low – about 0.1 (Watterson and Raghunathan, 1996). This gives a high Reynolds number and means that they must be of a reasonably large radius. Torque from the turbine pulsates at twice wave frequency due to the oscillating nature of the device; the power delivery can be smoothed by allowing the turbine speed to vary over a cycle so that kinetic energy is stored in the turbine/generator inertia as the speed increases and then converted to electrical energy as it slows. The Limpet OWC on The Isle of Islay, UK (see Wavegen Ltd. website in references) uses a cage induction generator via a controlled rectifier (to magnetize the generator), DC link and inverter, and this is a common arrangement for this device.

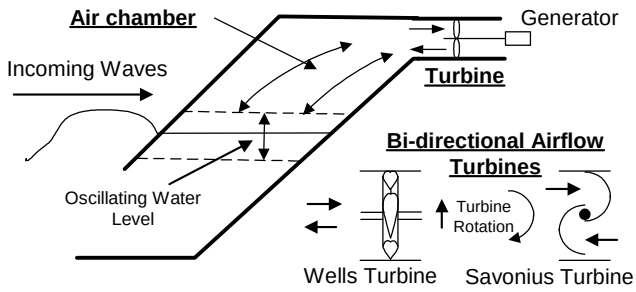

Fig. 1. Oscillating water column arrangement with oncoming waves

OWCs are suitable for use on shoreline locations as well as near-shore locations. The wave resource is often low or of poor quality when the sea shallows (Tucker and Pitt, 2001). Indeed, some locations will have very poor quality waves and the wave fronts will be of limited length and also may not be oncoming on to the front of the column. One way round this is to use a segmented OWC as shown in Fig. 2 (Dorrell and Hsieh, 2007). This could represent a system designed for a harbour wall where the wave fronts travel across the front of the column rather than oncoming into the column front face. For effective operation the width of each section needs to be somewhat less than the wave length. This requires either separate turbines for each section or a cascaded turbine structure (the figure shows three sections and three series-connected Savonius rotors). This decouples the internal oscillating water height in each other and to some extent will aid the smoothing of the power

delivery to the turbine generator if sections are oscillating in different phases. The effect of non-parallel oncoming waves will be further investigated here were the same OWC chamber is used but the three sections are merged into one so that a single Wells turbine can be used. However, since the wave run across the face of the column, shorter wave lengths may not produce substantial internal water oscillation.

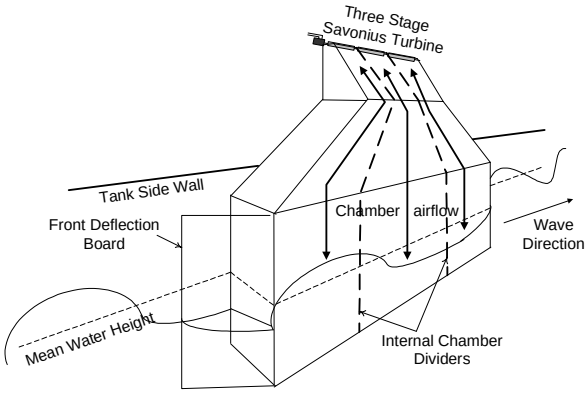

Fig. 2. Three-segment OWC with waves travelling across the column front face

Paper Outline

The paper will also report on the assessment of the integration of a demonstrator Wells turbine into a system. It will begin with a study using computational fluid dynamic analysis (using CFX software) of the double-stage turbine. The analysis is carried though to assess performance under reciprocating airflow conditions. These show that the energy conversion is quite low due to a low Reynolds number (Setoguchi *et al*, 2000). By use of variable pitch blades it is possible to obtain better performance and this is illustrated using the CFD. In addition, results are put forward for a scaling-up exercise – this shows the increasing performance of the Wells turbine with size and illustrates the need for a high Reynolds number.

Experimental data will be put forward from the mounting of the turbine on a small-scale oscillating water column. The turbine is connected to a DC machine to act as the generator for the system. Because the system is very low power then system has to be characterized so that losses and performance can be carefully assessed. In this way then the generating performance of the turbine can be obtained by measurement of the DC machine voltage and current as well as the turbine speed.

The power delivery is low so that the turbine speed remains almost constant over the cycle of a wave. Hence a simple load consisting of a power supply and parallel resistances (to dissipate power if the turbine/generator does begin to generate) can be used (this is described later). However, in a system with a large turbine the speed will oscillate with wave period. To maintain speed and allow some controlled speed variation within the airflow oscillating cycle, speed feedback and a DC/DC chopper is required.

The tank itself will allow waves with quantified periods and heights to be generated. This allows the OWC to be properly characterized and the results from the experiments are compared to the CFD predictions to corroborate the simulations.

MATLAB programmes are used to solve the system equations and to model the system. This allows for further investigation of the losses and gives an insight into a method of complete system simulation using modern software tools.

The paper will therefore report an a full analysis of a small oscillating water column system which includes CFD analysis of the turbine, performance of the OWC and design and development of the electrical system necessary for controlling and harvesting the energy on a small demonstrator unit.

Experimental Arrangement

For a small experimental wave-tank-scale set-up something simple like a Savonius rotor can be used (Dorrell and Hsieh, 2007) as shown in Fig. 2. However, larger systems use Wells turbines (Savonius rotors have a very limited conversion rate though work down to small sizes) and we can use a small one (although the conversion rate is expected to be low). The double -stage turbine is shown in Fig. 3. It has an outer diameter of about 132 mm and a centre hub diameter of 74 mm.

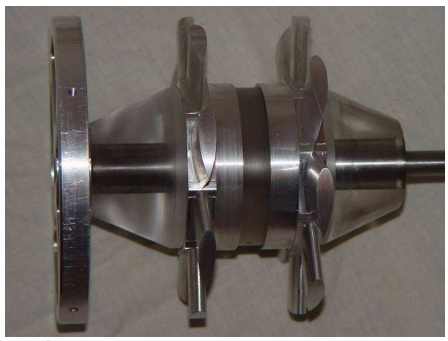

Fig. 3. Wells turbine

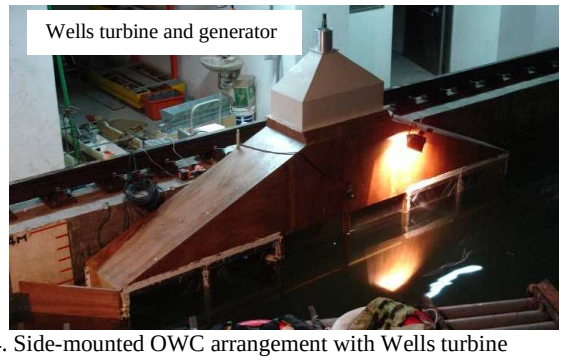

Fig. 4. Side-mounted OWC arrangement with Wells turbine

The turbine was relatively easy to manufacture and a permanent magnet generator can be used to develop a few watts of energy. It requires a flow coefficient of around 0.1 so that it rotates at either a high speed or low inlet velocity to maintain the flow coefficient. It will have a conversion rate of only a few percent and possibly not enough to overcome the friction and windage losses of the system for an oscillating airflow.

It was used in this application to illustrate the operation of a small column. This was fitted to a side-wall-mounted water column as shown in Fig. 4. This was originally three separate chambers but the top was modified to feed all the air through one Wells turbine (seen here mounted on the top with a small DC machine. The chamber is 4.5 m long when considering the three chambers together. If the wavelength is close to this then no pressure ***will*** be built up in the chamber and the water ***will*** not oscillate inside (or will oscillate out of phase such that air moves from chamber to chamber rather than pushed out through the turbine). This was done deliberately to assess the affect of column length in conjunction with the wavelength and a derivation is put forward below to take this into account.

COMPUTATIONAL FLUID DYNAMIC ANALYSIS OF THE WELLS TURBINE

The blades have a NACA15 profile and were manufactured within the

University of Glasgow. This a standard shape as used previously on Wells turbines (Raghunathan, 1995). In this section a study of the turbine is put forward using computational fluid dynamic analysis (package CFX)

The speed of the turbine was simulated as being either 1000 rpm or 1500 rpm. It was envisaged that prototype would not run above about 2000 rpm at the time of the CFD study although subsequent work found it possible to run safely up to 4000 rpm. The rotor was housed in a steel tube with roller bearings mounted at each end and supported using a spider mounting to allow airflow through it.

A commercial software package CFX 5 was used for the 3D simulation work. This is a general-purpose CFD program that uses a CAD based geometry/mesh pre-processor in conjunction with a physics pre-processor, which allows each individual section of a complex model to be appropriately meshed. It is split into five separate programs: Build, pre, solver, solver manager and post. CFX 5 uses the finite volume method. In this technique the flow field is broken into a set of fluid elements (triangles for two dimensional problems and polygons for three dimensional problems) and the conservation equations for each of these elements are written in an appropriate form. From the conservation equations a set of algebraic equations are created and solved numerically for the flow field. The size, shape and number of fluid elements depend on the complexity of the flow region, for example, in areas of complex flow the concentration of elements increases to improve accuracy. Therefore, for complex geometries such as the Wells turbine there can be as many as eighty thousand fluid elements in a simulation. In CFX 5 the program automatically defines the number of elements at the meshing stage, but the user also has the option of increasing this number for areas of special interest.

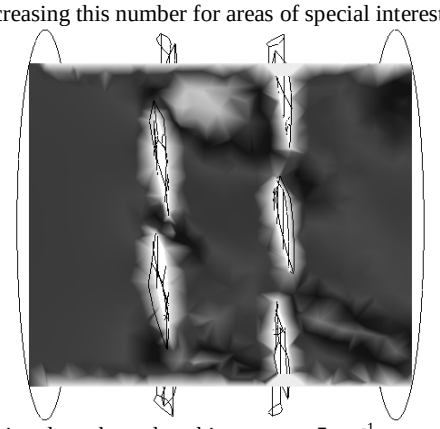

Fig. 5. Velocity plane through turbine rotor at 5 ms^{-1}

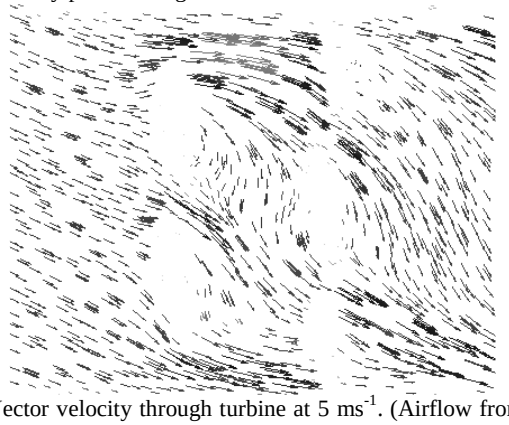

Fig. 6. Vector velocity through turbine at 5 ms^{-1}. (Airflow from left to right and the two-stage blades are rotating in the upward direction)

The models are three dimensional and represent the flow through the turbine from the inlet to the outlet. The pressure at the inlet is a relative pressure. The outlet pressure is set to zero though in reality it would be normal air pressure at sea level. The air density at the inlet was set to air density at 20°C and sea level. From the oscillating water column dimensions, turbine inlet diameter and the wave-height, the maximum flow rate through the turbine was estimated to be a maximum of about 10 ms^{-1}. Once the models were built up then various simulations could be run. Fig. 5 illustrates the cylindrical contour that was taken through the turbines to inspect the flow velocity vectors, as illustrated in Fig. 6. Streamlines could also be inspected as shown in Figs. 7 and 8 (Fig. 8 is for an earlier single-stage design). Space constraint prevents the illustration of many of the flow velocity vector plots and also the streamline plots.

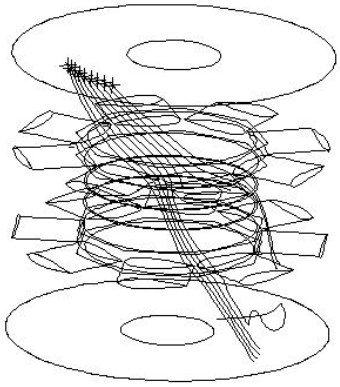

Fig. 7. Streamline plot through second turbine rotor at 5 ms^{-1}

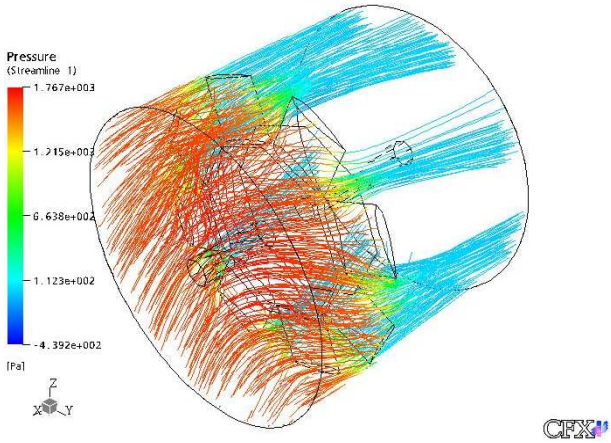

Fig. 8. Different streamline aspect plot (with single stage turbine rotor)

The input power can be calculated using the input air velocity and inlet pressure. The pressures and airflow velocities in this application are relatively low. The inlet power can be obtained from

$$P_{in} = P_{pressure} + P_{kinetic} \tag{1}$$

where

$$P_{pressure} = \text{inlet pressure} \times \text{inlet velocity} \times \text{inlet cross-sectional area} \tag{2}$$

and the inlet cross-sectional area is the area enclosed by the rotor diameter minus the area enclosed by the rotor hub. Also

$$P_{kinetic} = \frac{\text{mass flow rate} \times (\text{inlet velocity})^2}{2} = \frac{\rho_{air} \times \text{inlet cross-sectional area} \times (\text{inlet velocity})^3}{2} \tag{3}$$

The output power can be calculated from the torque (automatically calculated in CFX 5 in the simulations) and turbine speed.

Constant Flow Results

The turbine was modelled and the performance obtained at 1000 rpm and 1500 rpm at different steady-state inlet airflow velocities. The results are shown in Figs. 9 and 10 for the variation of output power and conversion factor with inlet velocity. More power is generated at higher velocities as expected but the conversion factor is still poor and it peaks at 1.4 % at an inlet velocity of 7 ms^{-1}.
The Reynolds number is given by

$$\mathbb{R} = \frac{uX}{v} \tag{4}$$

where u is the velocity of the flow, X is the characteristic length (pipe diameter – boss diameter) and v is the kinematic viscosity of the fluid (for dry air at 20°C = 15.1×10^{-6} m^2s^{-1}). For this turbine the Reynolds number is $u\times7.61\times10^3$ so that the velocity through the turbine needs to be calculated. At 10 ms^{-1}, the Reynolds number is 0.76×10^5 which is low for this sort of turbine, and often the peak inlet airflow velocities do not reach this level. Generally this type of turbine operates successfully when the Reynolds number is in the region of 10^6. To test this, a later section reports on simulations where the diameter is increased by five and the maximum inlet airflow velocity is increased to 50 ms^{-1}. This puts the Reynolds number up into this region.

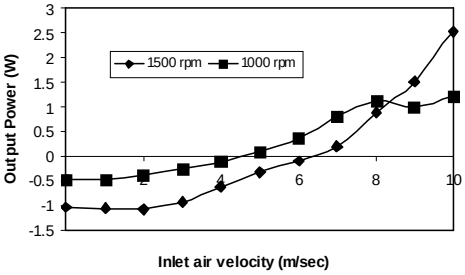

Fig. 9. Output Power variation with constant inlet air velocity

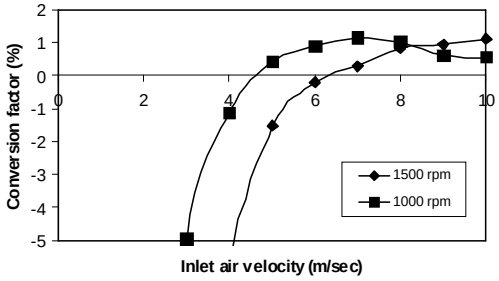

Fig. 10. Conversion rate variation with constant inlet velocity

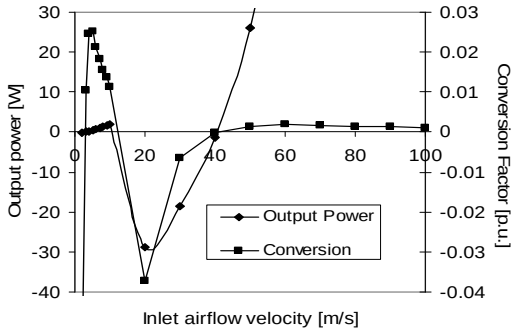

Fig. 11 Extended inlet flow range at 1000 rpm

Another design issue that has to be considered is the tip velocity to inlet airflow velocity ratio. For this type of turbine the tip velocity to inlet airflow velocity ratio should be about ten (the inverse of this is called the flow coefficient which should be about 0.1 for good operation, Watterson and Raghunathan, 1996), so when we scale the turbine up we can also increase the inlet airflow velocity. However, using this small turbine we can increase the inlet velocity to try and increase the Reynolds number. In Fig 11 this was done but unfortunately this increases the flow coefficient and the stall point was reached at about 15 ms^{-1} for 1000 rpm which is a tip to inlet velocity ratio of 0.50 (flow coefficient of 2). When the turbine is scaled then the inlet airflow velocity is also scaled up to maintain a constant tip to inlet velocity ratio, this is investigated later. While at output power at an inlet flow of 100 ms^{-1} is 1.2 kW, this is actually only 0.1 % conversion and an unrealistic operating point. When the streamlines are inspected then it is found that, due to the extremely high inlet velocity, the streamlines stop at the blades; thereby indicating low aerodynamic but high pressure forces. This illustrates that to obtain good results either the turbine speed needs to be increased, or the turbine cross section. It is found that the real solution is the latter case as will be illustrated later.

Oscillating Airflow Operation

The variation of generated power with oscillating inlet airflow velocity is shown in Fig. 12 and the mean power from the oscillating airflow is shown in Fig. 13 for comparison to the fixed-flow turbine rotor results. The performance is affected by the oscillating airflow as can be seen in the figures. Fig. 12 uses the steady flow results to reconstruct a waveform for the power over one cycle of a wave. The wave normally has a time period of several seconds so this is assumed to be a reasonable approximation. For the oscillating airflow then it is the peak airflow that is denoted rather than constant airflow.

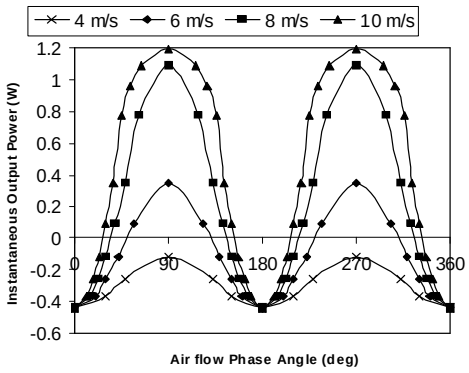

Fig. 12. Variation of instantaneous output power with airflow

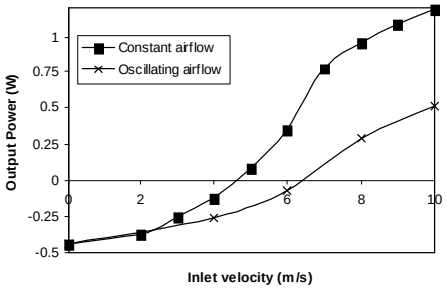

Fig. 13. Comparison between fixed flow and oscillating flow conversion rates

Swivelling Blade Operation

The simulation work seems to suggest that the turbine is simply too small though it does represent an interesting academic investigation. A model was developed with rotating or swivelling blades to see if this could produce improved performance and overcome the problems

associated with the small turbine size. The results from this study are shown in Figs. 14 and 15 for the output power and conversion factor. At about 4 degrees there is a great improvement in the generator power but the conversion rate is still only peaking with 7.4 % at 5 ms^{-1} which then decreases to 3.8 % at 10 ms^{-1}. The peak output power occurs at 6 degrees and then decreases at 8 degrees. It appears that the band for peak performance is quite narrow with a sharp rise in output power between 2 and 4 degrees of rotation then a fall in output power between 6 and 8 degrees of rotation

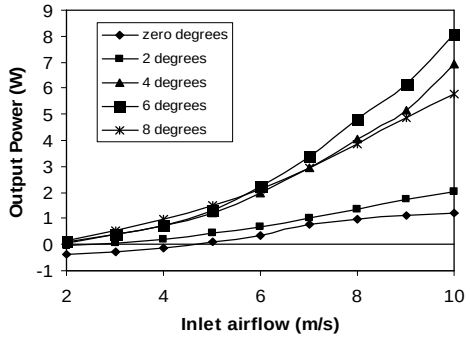

Fig. 14. Output power variation with swivelling blades at 1000 rpm

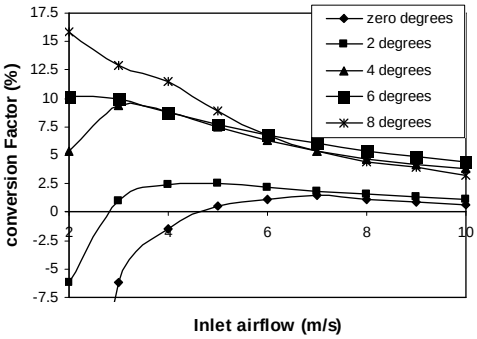

Fig. 15. Conversion factor variation with swivelling blades at 1000 rpm

Enlarged Machine Simulation

Generally this type of turbine operates successfully when the Reynolds number is in the region of 10^6. To test this, simulations were conducted where the diameter is increased by five and the maximum inlet airflow velocity is increased to 50 ms^{-1}. This puts the operating Reynolds number up into this region.

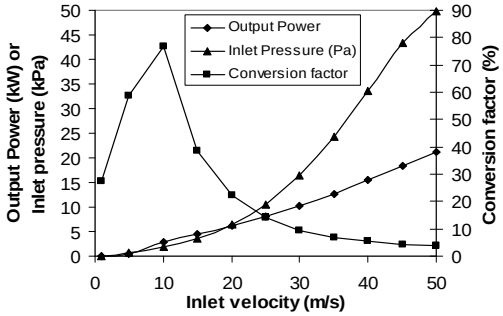

Fig. 16. Output power, conversion factor and inlet pressure for enlarged turbine at 1000 rpm

The turbine was scaled up so that the rotor diameter is now 660 mm and the speed scaled to 50 ms^{-1}. We now obtain an almost linear range when comparing the output power to the inlet airflow velocity as illustrates in Fig. 16. These results were obtained at 1000 rpm and constant inlet airflow. The rating of this turbine then appears to have a suitable rating up to about 10 kW (peak), where the conversion rate decreases to about 10 %. Above this point the water column could be too large because the efficiency is low. The peak efficiency is at 10 ms^{-1} inlet airflow which is 77 % and a flow coefficient of 0.27. This may seem high but it is with constant airflow. If we allow the water to oscillate then we can get the conversion rate over one airflow cycle (Fig. 17) which will be in the range of about 40 % at 3.6 kW (both average over one cycle with a peak flow of ± 20 ms^{-1} and pressure of ± 6.5 kPa around an air pressure of 101.3 kPa) and 30 % at 5.9 kW (again both average over one cycle, and a peak airflow of ± 30 ms^{-1} and pressure of ± 16.4 kPa). These put the overall efficiencies in the range of large turbines previously constructed. For the turbine installed in the Islay plant, the turbine is a contra-rotating type with two sets of turbine blades, each set consisting of seven blades (NACA12 profile) and a rotor diameter of 2.6 m. The rated speed is 1050 rpm at pressure oscillation of ± 9 kPa across the two stages, although it could rise much higher than this. The generator is rated at 250 kW. If the overall conversion rate is about 40 % (an estimate) then, with a hub-to-tip diameter ratio of 0.62, the inlet velocity is calculated to be 80 ms^{-1}.

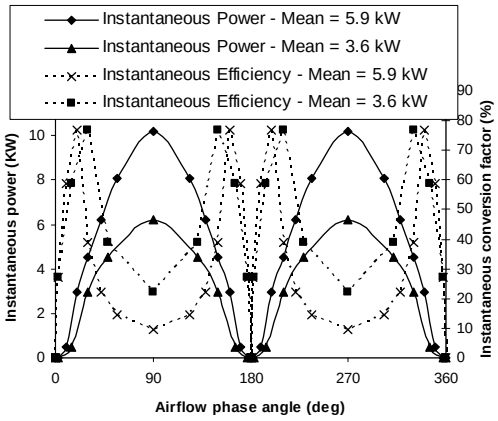

Fig. 17. Instantaneous power and efficiency for enlarged turbine at 1000 rpm

OWC AND WAVE TANK STUDY

The OWC was tested in a wave tank. This tank had a range of available waves but it was decided to use waves with 2.8 s and 4 s periods. The wave heights were maximum for the 2.8 s period but operation was still possible for the 4 s period. In addition to these periods a 2 s period was also investigated to assess the influence of wavelength.

In this section the chamber performance is first assessed then the performance of the turbine in conjunction with chamber. Equations derived in Dorrell and Hsieh, 2007 are implemented to assess the performance.

Chamber and Wave Performance

The chamber is 4.5 m long and the waves go across the face of this. Because a Wells turbine is used then the wave height will vary across the face of the device. In the study in Dorrell and Hsieh this was divided into three but here the chambers were merged at the top to feed the turbine. Therefore air is free to move between one chamber and another. Hence it is necessary to address the wave length of the waves. The depth of the tank was about 3.35 m. This is really an intermediate water depth (Boyle, 1996). In deep water the wavelength L_0 is given by

$$L_0 = \frac{g}{2\pi f^2} = 1.56T^2 \quad \text{m} \tag{5}$$

where T is the wave period. Boccotti, 2000, gives an expression for the

reduction of wavelength due to decreasing depth:

$$L \cong \left(1-\frac{\pi d}{3L_0}\right)T\sqrt{gd} \tag{6}$$

where d is the water depth and g is gravity. In the experiments, the wave period varied from 2 s to 4 s. Implementation of (5) and (6) leads to the characteristics shown in Table 1. These illustrate the reduction in wavelength and it can be seen that the 2 s period gives a wavelength similar to the chamber length. When the system was run it was found that levels in the chambers were in phase with the passing wave and out of phase with each other by a suitable phase so that air appeared to move between chambers but little air passed through the turbine and no measureable generation appeared.

Table 1. Calculated wavelengths for wave tank

	Wave period T [s]		
	2	2.8	4
Deep water wavelength L_o	6.24 m	12.23 m	24.96 m
Wave tank wavelength L	5.02 m	11.44 m	19.70 m

If the oscillating water column is L_C m long then the mean wave height across the face of the column (for a peak height H) is given by

$$x_0(t) \approx \frac{H}{2}\cos\left(\frac{2\pi}{T}t\right)\times\frac{1}{\theta}\int_{-\theta/2}^{\theta/2}\cos(\phi)d\phi = \frac{H}{2}\cos\left(\frac{2\pi}{T}t\right)\times\frac{2\sin\left(\theta/2\right)}{\theta} \tag{7}$$

where $\theta = 2\pi \times L_C / L$. If the wave period is 2.8 s then the wavelength is 11.44 m $\theta = 2\pi \times 4.5/11.44 = 0.76\pi$ so that

$$x_0(t) \approx \frac{0.8H}{2}\cos\left(\frac{2\pi}{T}t\right) = X_0\cos\left(\frac{2\pi}{T}t\right) \tag{8}$$

For the calibration wave, T = 8 s, so that the wavelength is 44 m using equations (5) and (6), then $\theta = 2\pi \times 4.5/44 = 0.20\pi$ giving a mean wave height of X_0 = 0.98H/2. For further wave heights, T= 4 s the wave length is 19.70 m so that the mean height in the column is X_0 = 0.92H/2 and T = 2 s gives X_0 = 0.11H/2 which shows that there is virtually no mean oscillation in the column. This illustrates the attenuation of the performance of the OWC with increasingly shorter wavelengths.

Once the mean wave height across the face of the column is obtained then the mean water height has to be calculated for inside the column. The water height inside the oscillating water column can be approximated to:

$$x_1(t) \approx K_1 X_0 \sin\left(\frac{2\pi}{T}t\right) \tag{9}$$

From Dorrell and Hsieh, 2007:

$$x_1\frac{\partial^2 x_1}{\partial t^2} + \left(\frac{\mathrm{d}x_1}{\mathrm{d}t}\right)^2 + f\left(\frac{\mathrm{d}x_1}{\mathrm{d}t}\right) - g(x_0 - x_1) = 0 \tag{10}$$

And the function (corrected from Dorrell and Hsieh, 2007):

$$f\left(\frac{\mathrm{d}x_1}{\mathrm{d}t}\right) = \frac{\Delta p}{\rho_s} = \frac{p_1 - p_0}{\rho_s} \tag{11}$$

Where p_1 is the pressure on the surface of the column water, p_0 is air pressure and ρ_s is the density of sea water. The pressure on the air surface can be related to the pressure at the turbine from

$$p_1 \approx p_2 - \frac{1}{2}\rho\left(V_1^2 - V_2^2\right) = p_2 - \frac{1}{2}\rho V_1^2\left(1-\left(A_1/A_2\right)^2\right) \tag{12}$$

Where V_1 is the velocity of the water surface and V_2 is the air velocity in the turbine, A_1 and A_2 are the column water surface area and the cross section of the turbine, and ρ is the density of air. From the CFD analysis the pressures were noted against the airflow. These gave the characteristics shown in Fig. 18 and this gives the equation

$$p_2 - p_0 = 24.8V_2^2 - 40.68V_2 = 24.8\left(\frac{A_1}{A_2}\right)^2 V_1^2 - 40.68\frac{A_1}{A_2}V_1 \tag{13}$$

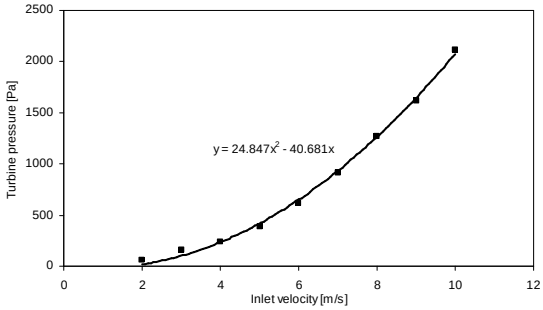

Fig. 18. Turbine pressure against inlet velocity for Wells turbine

Combining (12) and (13) and putting into (11)

$$f\left(\frac{\mathrm{d}x_1}{\mathrm{d}t}\right) = \frac{p_1 - p_0}{\rho_s}$$
$$= \frac{1}{2}\left(\frac{\mathrm{d}x_1}{\mathrm{d}t}\right)^2\frac{\rho}{\rho_s}\left(1-\left(A_1/A_2\right)^2\right) + \frac{24.8}{\rho_s}\left(\frac{A_1}{A_2}\right)^2\left(\frac{\mathrm{d}x_1}{\mathrm{d}t}\right)^2 - \frac{40.68}{\rho_s}\frac{A_1}{A_2}\frac{\mathrm{d}x_1}{\mathrm{d}t} \tag{14}$$

This can be combined with (10) and programmed using the Runge-Kutta method. This is similar to the method used in Dorrell and Hsieh, 2007, but includes the function for the water velocity in (14) which is the turbine pressure term. However under steady-state sinusoidal operation, and neglecting higher harmonics:

$$\frac{40.68}{\rho_s}\frac{A_1}{A_2}\frac{\mathrm{d}x_1}{\mathrm{d}t} + g(x_0 - x_1) \approx 0 \tag{15}$$

$$x_1 = \frac{gX_0e^{j\omega t}}{g - j\omega\dfrac{40.68}{\rho_s}\dfrac{A_1}{A_2}}$$
$$= \frac{9.8X_0e^{j\omega t}}{9.8 - j\dfrac{2\pi}{T}\dfrac{40.68}{1030}\dfrac{2.25}{0.0137}} = \frac{9.8X_0e^{j\omega t}}{9.8 - j\dfrac{40.8}{T}} \tag{16}$$

When T = 2.8 s then the attenuation for the internal wave height will be due to the attenuation due to the wavelength and also attenuation due to the small turbine aperture so $0.8 \times 0.56 = 0.45$. When the wave period is 4 s then the internal wave height will be $0.92 \times 0.56 = 0.64$. These are approximations but do include the pressure terms.

During the experiments using the wave probes, it was found that the probes were integrating so that their output had the function of x = 6.25HT on the scope settings used. The chamber water height and wave height were calibrated together using small waves of long period so that the levels oscillated together. The chamber water height at 2.8 s and 4 s were attenuated while at 2 s the levels were the same because the wavelength is only slightly longer than the chamber which is divided into three at water level so that air moves from one chamber to another rather than cycling in and out through the turbine under pressure. However, 2.8 s gives 0.38 attenuation, while 4 s gives 0.57 attenuation from outside to inside the chamber; these can be compared to the predictions above, which show less than a 20 % error from prediction. This seems to be excellent given the approximations used in the method. There was considerable variation on the wave height measurements due to interference in the wave probe signals from the wave generating servo motor drives. Therefore they were obtained quickly at the end of a test during the period when the wave generator was switched off and the final wave passed the wave device.

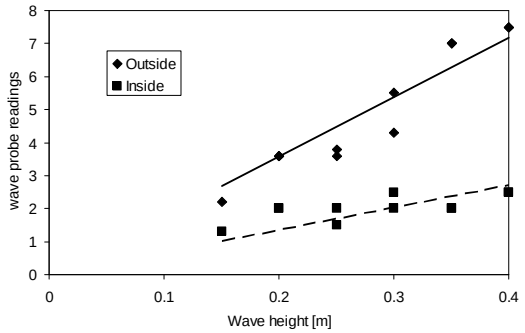

Fig. 19. Wave probe measurements for T = 2.8 s

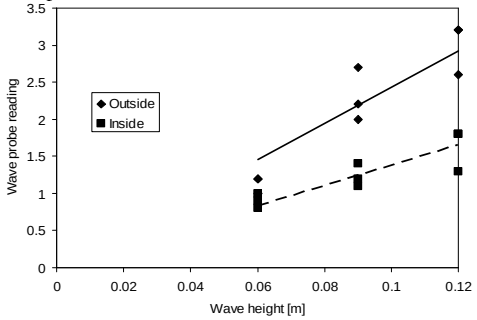

Fig. 20. Wave probe measurements for T = 4 s

Wells Turbine and Generator Characterisation

To test the system then the Turbine and generator need to be characterised. The turbine is connected to a permanent-magnet DC machine (Fig. 21). The DC machine can be characterised by carrying out a locked rotor test (to obtain R_a and V_b) and open circuit test (driving the machine and measuring the open-circuit terminal voltage) to obtain the back-EMF constant E_a. From these tests it was found that the brush drop voltage was 0.4 V and the armature resistance was 10.35 Ω. The machine constant K_E was found to be 0.0375 Vs/rad. The performance of the system can now be assessed by simply measuring terminal voltage and current and ensuring that the parameters do not drift with temperature or operation.

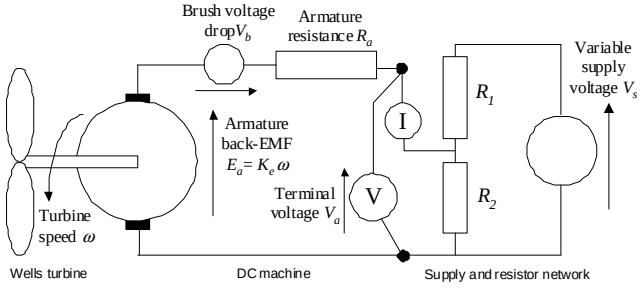

Fig. 21. Turbine/DC machine electrical connection

A no-wave motoring test was carried out to obtain the friction and windage of the system. The results are shown in Fig 22. This was obtained by back calculation for the terminal voltage and input current and calculating $E_a I_a$ (which is the mechanical input power). This gives a friction and windage power of $P_{fr} \approx 0.35\times10^{-6}N^2$ where N is the speed in rpm. This is used to calculate the turbine power by using the power difference. This test was repeated during the tests for 2.8 and 4 s waves. The power available at the turbine inlet was estimated in order to estimate the conversion rate. From Dorrell and Hsieh, 2007, the total mechanical power available at the turbine is due to the pressure drop and the kinetic energy:

$$P_{\text{total}} = \left(P_t + P_a\right) = \left\{ \begin{pmatrix} \rho \frac{A_1}{A_2}\left[-\frac{\left(X_0\omega\right)^2}{2}\left(2\cos\left(\omega t\right)^2 - 1\right)\right] \\ +\rho\frac{Q}{A_2}\left(V_2 - V_1\right) \end{pmatrix} + \frac{1}{2}\rho V_2{}^2 \right\} Q \quad (17)$$

where the equation of continuity is

$$Q = V_1 \times A_1 = V_2 \times A_2 \quad (18)$$

This assumes that the water level inside the column has the same height as the wave, however, as the water level decreases, decreasing the kinetic energy, the pressure increases for a given chamber water height in a corresponding manner, so (17) should not be a bad approximation. The equation is programmed over one cycle and the mean power calculated.

The system was tested with varying wave heights. The estimated power is taken as the difference in power when there are waves and when there are no waves. At 2.8 s and wave height of 0.4 m the waves have a power of about 440 W/m while the possible energy in the OWC at the turbine is 735 W. At 4 s and wave height of 0.12 m then the wave power is 56 W/m and the internal power at the turbine is 30 W. This illustrates that the column size and geometry should be selected to match a range of waves. At a period of 2 s there was negligible power.

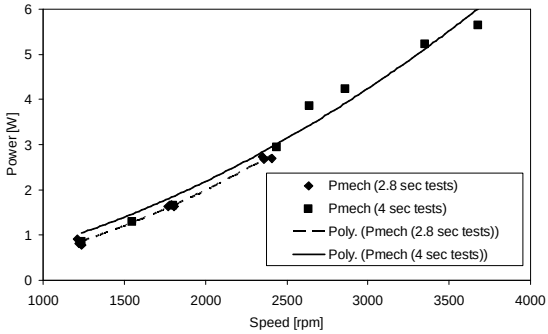

Fig. 22. Mechanical power against speed with no waves.

OWC Performance with Waves

The performance of the OWC is given in Figs. 23 to 28. Because the conversion rate is very low the turbine settled to a constant speed during operation with little speed oscillation. The tests were carried out at 2.8 s and 4 s wave periods and they show the generated power (difference in mechanical power between no waves and waves) against flow coefficient and conversion rate and then mean flow coefficient against conversion rate. In the CFD work the conversion rates appear to plateau at about 1 % conversion for 1000 rpm and 1500 rpm when the flow coefficients were about unity. In Fig. 25 it can be seen that this is about 0.4 % (by inspection of the 1448 and 1530 rpm points in Fig. 23). However, in Figs. 27 to 29 it can be seen that the conversion rates are higher for the 4 s wave periods because the flow coefficients are lower (although the output power is lower since the waves were smaller).

These results exclude the turbine friction and windage losses. In reality the conversion rates will be lower at high speed where the losses are high (Fig. 22). This emphasises that a larger diameter turbine is needed for this application. This is underpinned by Fig. 28 which combines the conversion rate against flow coefficient for both wave periods since results are for different points on the curve. It can be seen that the conversion rate does indeed increase greatly when the flow coefficient drops to about 0.1 which is in line with previous literate (Watterson and Raghunathan, 2006, and others).

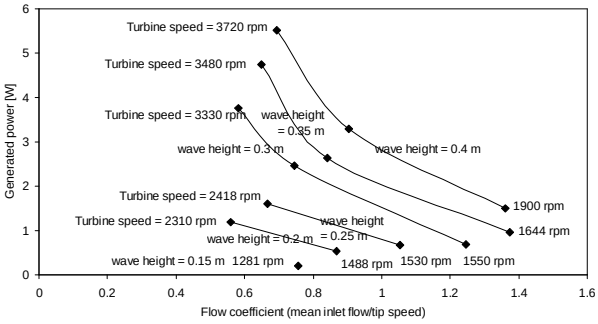

Fig. 23. Generated power against flow coefficient for 2.8 s waves

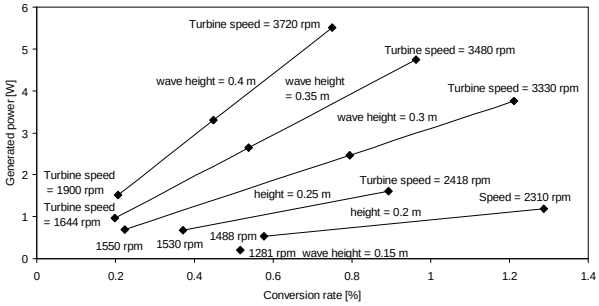

Fig. 24. Generated power against conversion rate for 2.8 s waves

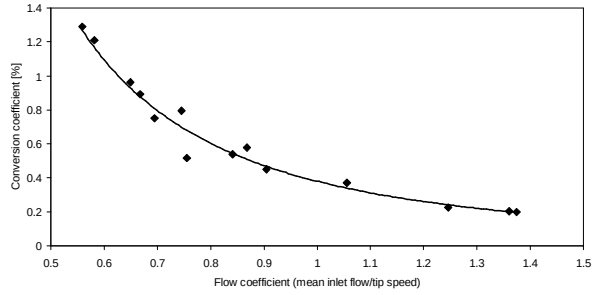

Fig. 25. Conversion coefficient against flow coefficient for 2.8 s waves

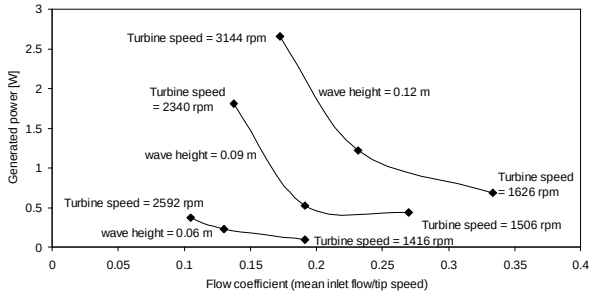

Fig. 26. Generated power against flow coefficient for 4 s waves

CONCLUSIONS

This paper reports on a computational fluid dynamic study on a small Wells turbine then goes on to examine its behaviour when fitted to an oscillating water column. The column behaviour is also studied and it is found that the turbine's performance was in line with the CFD simulations. While the turbine was a small demonstrator unit the work illustrates the procedure and design calculations that can be carried out in order to build a larger OWC and turbine with more practical performance. The work highlights the need to keep the turbine Reynolds number high while limited the flow coefficient to about 0.1. This paper illustrates that an OWC is predictable and a few design principles and calculations can be applied to develop a system.

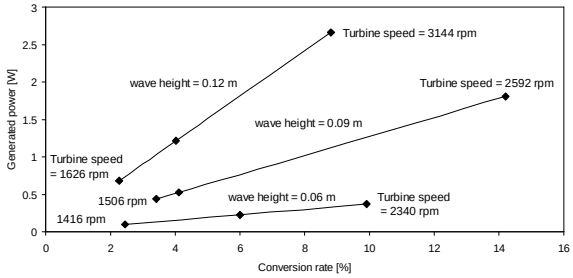

Fig. 27. Generated power against conversion rate for 4 s waves

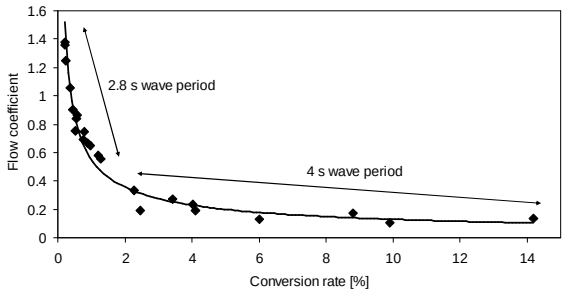

Fig. 28. Conversion rate against flow coefficient for 2.8 and 4 s waves

ACKNOWELDGEMENT

The authors are very grateful to Mr Martin Findlater who carried out the CFD work using CFX as part of his MEng project under the supervision of Dr Dorrell. The authors are also grateful to the Tainan Hydraulics Laboratory, NCKU, for financial support for the project.

REFERENCES

J. R. Halliday and D. G. Dorrell, "Review of Wave Energy Resource and Wave generator Developments in the UK and the Rest of the World", *IASTED EuroPES conference*, Rhodes, 28-30 June 2004.

D. G. Dorrell and M.-F. Hsieh, "Segmented small oscillating water columns using in-line Savonius rotors", *ISOPE Conference 2007*, Lisbon, Portugal, 1-6 July, 2007.

A. Clement, P. McCullen, A. Falcao, A. Fiorentino, F. Gardner, K. Hammarlund, G. Lemonis, T. Lewis, K. Nielsen, S. Petroncini, M.-T. Pontes, P. Schild, B.-O. Sjostrom, H.C. Sorensenaan and T. Thorpe., *"Wave Energy in Europe: current status and perspectives"*, *Renewable and Sustainable Energy Reviews* Vol. 6, Elsevier Science Publishers, pp 405-431, 2002.

J. K. Watterson and S. Raghunathan, "Investigation of Wells turbine performance using 3-D CFD", *Energy Conversion Engineering Conference, IECEC 96. Proceedings*, Washington, USA, Vol 3, pp 1777-1782, 11-16 Aug 1996.

Wavegen: http://www.wavegen.co.uk/what_we_offer_limpet_islay.htm

M.J. Tucker and E.G. Pitt, *Waves in Ocean Engineering*, Elsevier Publishers, Ocean Engineering Series, 2001.

T. Setoguchi, S. Santhakumar, M. Takao, T. H. Kim, K. Kaneko, "Effect of guide vane shape on the performance of a Wells turbine", *Renewable energy*, July 2000.

S. Raghunathan, "The wells air turbine for wave energy conversion", *Progress in Aerospace Sciences*, Vol 31, No 4, pp 335-386, 1995.

G. Boyle, *Renewable Energy, Power for a Sustainable Future*, The Open University, Oxford University Press, 1996, UK.

P. Boccotti, *Wave Mechanics for Ocean Engineering*, Elsevier Oceanography Series No. 64, 2000.